STAFF SUMMARY SHEET

	TO	ACTION	SIGNATURE (Surname), GRADE AND DATE		TO	ACTION	SIGNATURE (Surname), GRADE AND DATE
1	DFAN	sig	[signature] Col, 9 Mar 12	6			
2	DFER	approve	Brent A Rucker Col 12 Mar 2012	7			
3	DFAN	action	[signature] C1C 09 Mar 12 C1C Beau Stegemann	8			
4				9			
5				10			

SURNAME OF ACTION OFFICER AND GRADE	SYMBOL	PHONE	TYPIST'S INITIALS	SUSPENSE DATE
C1C Stegemann	DFAN	333-6836	bjs	20120315

SUBJECT		DATE
Clearance for Material for Public Release	USAFA-DF-PA- 101	20120309

SUMMARY

1. PURPOSE. To provide security and policy review on the document at Tab 1 prior to release to the public.

2. BACKGROUND.
Authors: C1C Joshua Moore, C1C Beau Stegemann,

Title: Comparison of Williams International WJ24-8F Uninstalled and Installed Performance

Circle one: Abstract Tech Report Journal Article Speech (Paper) Presentation Poster
Thesis/Dissertation Book Other: _____

Check all that apply (For Communications Purposes):
[] CRADA (Cooperative Research and Development Agreement) exists
[] Photo/ Video Opportunities [] STEM-outreach Related [] New Invention/ Discovery/ Patent

Description: This project characterized the performance of an uninstalled Williams International WJ24-8F with and without a bell mouth inlet, and compared the results with data from tests of the engine installed in the Northrop Grumman BQM-74E Chukar III aerial target drone, and the manufacturer's published engine performance.

Release Information: To be presented at the AIAA Student Paper Competition, Boulder CO, April 04-06, 2012

Previous Clearance information: (If applicable): None.

Recommended Distribution Statement: Distribution A: approved for public release, distribution unlimited

3. DISCUSSION.

4. RECOMMENDATION. Sign coord block above indicating document is suitable for public release. Suitability is based solely on the document being unclassified, not jeopardizing DoD interests, and accurately portraying official policy.

[signature]
Thomas E. McLaughlin, Ph.D.
Director, Aeronautics Research Center

Comparison of Williams International WJ24-8F Uninstalled and Installed Performance

Joshua Moore[a] and Beau Stegemann[b]
United States Air Force Academy, CO, 80840

K. Colin Tucker[c]
United States Air Force Academy, CO, 80840

This project characterized the performance of an uninstalled Williams International WJ24-8F with and without a bell mouth inlet, and compared the results with data from tests of the engine installed in the Northrop Grumman BQM-74E Chukar III aerial target drone, and the manufacturer's published engine performance. Over a series of five test runs, the performance was characterized to include parameters such as thrust, thrust specific fuel consumption, and air mass flow rate through the engine. These parameters were then compared to the installed performance recorded previously. The uninstalled engine with a bell mouth inlet was found to have a corrected thrust of roughly 260 lbs and a corrected thrust specific fuel consumption of roughly 1.15 lbm/hr. The uninstalled thrust performance was roughly 10% higher than the installed thrust. The increase in uninstalled thrust compared to installed thrust can be attributed to the inlet losses of the drone as well as the additive force from the bell mouth inlet. Specifically, the drone uses a serpentine inlet which is especially prone to losses due to separation. The uninstalled thrust with the bell mouth inlet was also found to be 8% higher than the published values and 5.9% higher than the thrust without the bell mouth inlet. When the thrust specific fuel consumption was compared, the uninstalled result during tests with the bell mouth inlet was 6.7% lower than without, 4.3% lower than the published value, and 17.5% lower than the installed value. The mass flow rate of air through the engine was also characterized across the RPM band in order to support, and set a foundation for, future research with this engine. Finally, differences in engine performance between the published data, installed tests, uninstalled tests without a bell mouth inlet, and uninstalled tests with a bell mouth inlet were examined for possible causes such as the nature of the engine's design, inlet losses, *vena contracta,* and bell mouth inlet pressure differential.

Nomenclature

a	=	speed of sound (ft/sec)
A	=	annular area (in^2)
B	=	bias Error
F_c	=	corrected uninstalled thrust (lb_f)
M	=	Mach number
$\dot{m}_f$	=	mass flow of fuel (lb_m/sec)
$\dot{m}_o$	=	mass flow of air (lb_m/sec)
N	=	uncorrected RPM (revolutions per minute)
N_c	=	corrected RPM (revolutions per minute)
P	=	precision error
P_o	=	observed static pressure (psi)

[a] C1C, Department of Aeronautics, P.O. Box 4305, AIAA Member
[b] C1C, Department of Aeronautics, P.O. Box 5221, AIAA Member
[c] Lt Col, Deputy of Operations, Department of Aeronautics, AIAA Senior Member

P_{ref} = atmospheric, sea level pressure (psi)
P_t = total pressure (psi)
R = gas constant ((ft*lb_f)/ (lb_m*R))
S = uninstalled thrust specific fuel consumption (lb_m/lb_f-hr)
S_c = corrected uninstalled thrust specific fuel consumption (lb_m/lb_f-hr)
T = installed thrust (lb_f)
T_o = observed static temperature (R)
T_{ref} = atmospheric, sea level temperature (R)
T_t = total temperature (R)
$TSFC$ = installed thrust specific fuel consumption (lb_m/lb_f-hr)
V = velocity (ft/sec)
γ = ratio of specific heats
ρ = density (lb_m/in^3)

I. Introduction

The United States Air Force Academy is constantly working in conjunction with Air Force unmanned aerial system research programs. As such, the Department of Aeronautics is in need of compact turbofan and turbojet engines for its research projects. In order to successfully utilize small scale turbojet engines in its research, the Air Force Academy must develop methods for both testing and evaluating small class engines. One such project, the Williams International WJ24-8F turbojet engine was examined in the Spring of 2011 as a possible engine for use in the United States Air Force Academy Department of Aeronautics' Campus 2.0 aerial target drone.[4] The WJ24-8F engine is a small scale turbojet engine capable of producing 240 lbs of thrust at sea level static conditions and was originally used in the Northrop Grumman BQM-74E Chukar III aerial target drone.[4] This drone is primarily utilized by the Navy to simulate aircraft threats. The drone has the ability to fly from 15 ft to 40,000 ft with a top speed of over 525 knots and can perform 6g maneuvers.[1] Also, the drone is designed to withstand numerous water landings; therefore, the WJ24-8F is designed to operate after subjected to thermal shock. Due to this requirement, the engine is overbuilt, and the manufacturer's specifications are characteristic of the performance at the end of the engine's life. When the WJ24-8F was originally evaluated, all data was taken with the engine mounted in the United States Navy's BQM-74E Chukar III remote controlled aerial target drone.[4] This particular drone utilizes a serpentine inlet due to design constraints on engine placement. While necessary for the Chukar III, the serpentine inlet design causes losses due to the flow direction changes. The inlet losses of the Chukar III resulted in a lower maximum thrust during testing than the published value. While the inlet losses changed the performance characteristics of the WJ24-8F the nozzle should not affect the installed versus uninstalled data since the nozzle is incorporated into the engine and does not vary with instillation. The primary focus of this project is to characterize the uninstalled performance characteristics of this engine in order to set a baseline for future Air Force Academy research projects, as well as further develop the methods used to test and evaluate small scale turbojets.

A. Previous Experimentation

A similar project was conducted in the Spring of 2011 in order to evaluate the performance of the Williams International WJ24-8F turbojet engine while installed in the United States Navy's BQM-74E remote controlled aerial target drone. This configuration is detailed in Figures 1, 2, and 3 below. During the evaluation of this engine the thrust, corrected thrust, TSFC, Mach number at the inlet, and mass flow through the engine were determined. Figures 4-7 depict these findings.

Figure 1. Installed Engine Setup

Figure 2. The WJ24-8F turbojet engine mounted to the BQM-74 Aerial Target Drone on a thrust stand in Test Cell #4

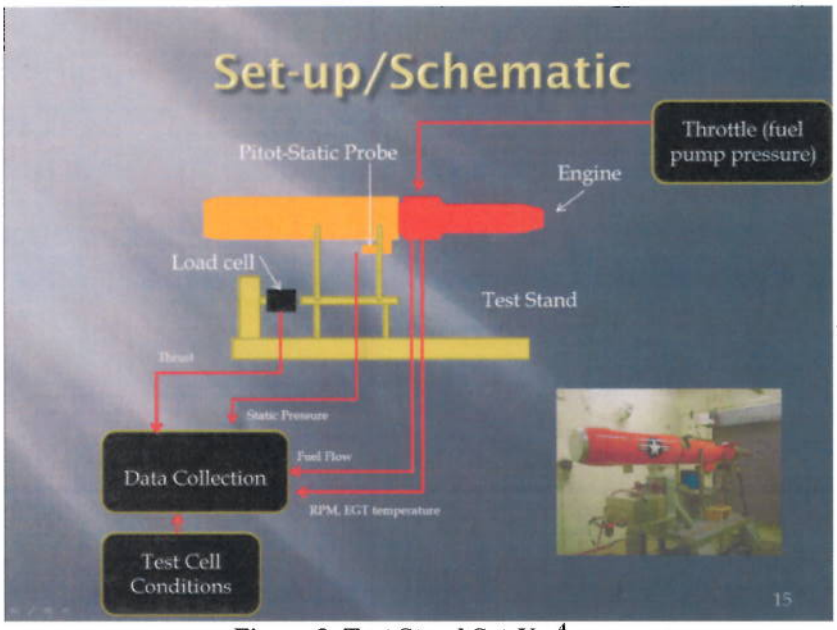

Figure 3. Test Stand Set-Up.[4]

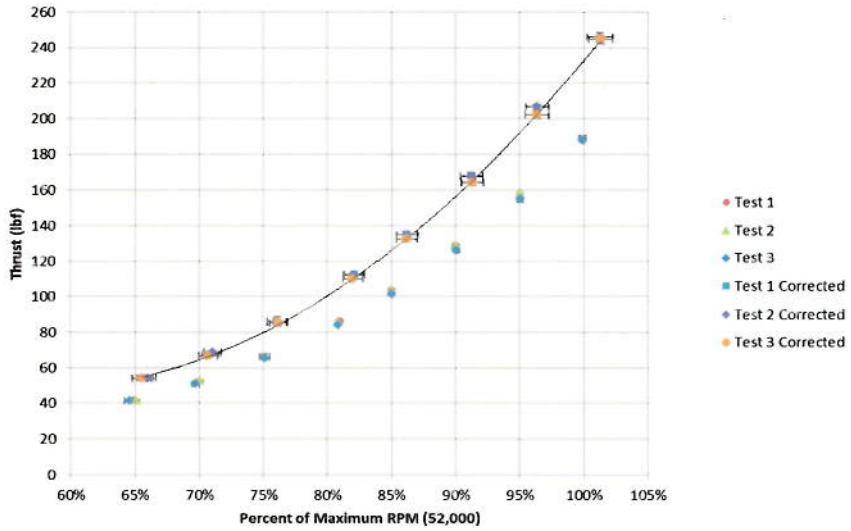

Figure 4. Uncorrected and corrected installed thrust versus uncorrected and corrected percent maximum RPM with error bars.[4]

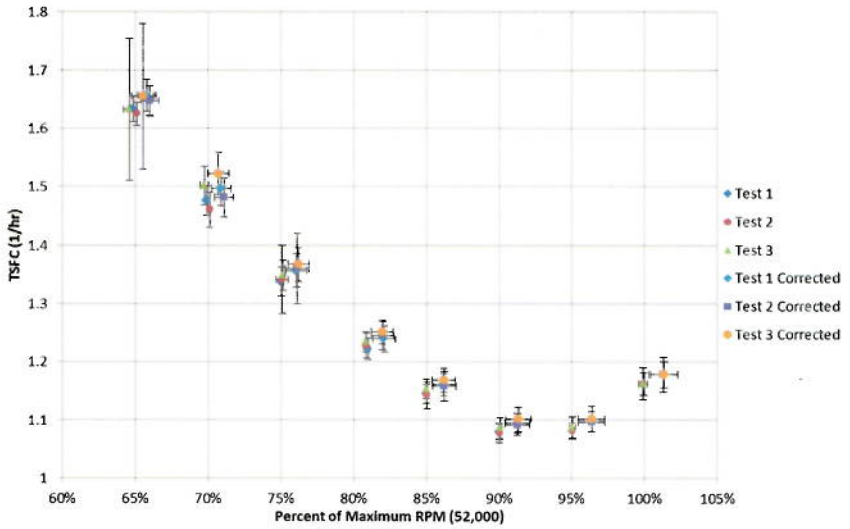

Figure 5. Uncorrected and corrected installed Thrust Specific Fuel Consumption versus uncorrected and corrected percent maximum RPM with error bars.[4]

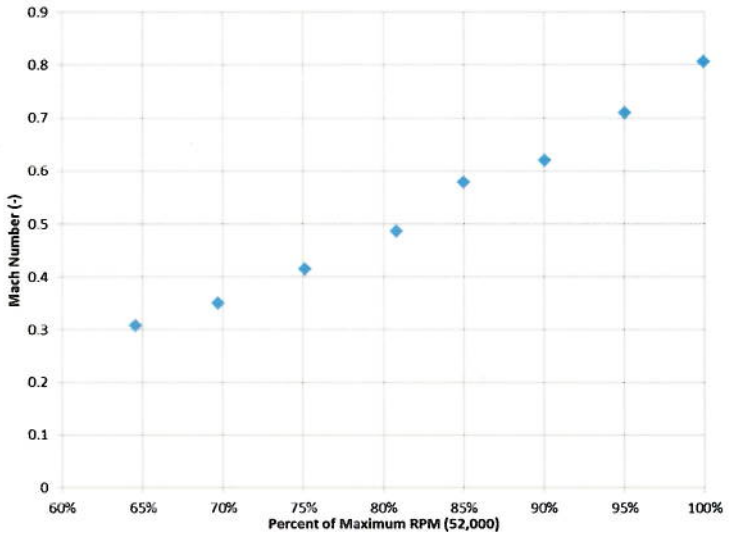

Figure 6. Installed inlet Mach number as a function of the percent of maximum RPM.[4]

Figure 6 above shows the inlet Mach number for the installed engine. This Mach number was calculated using a pitot-static probe placed in the inlet, and the following Equation 1seen below.

$$M = \sqrt{\frac{\left(\frac{P_t}{P_0}\right)^{\frac{\gamma}{\gamma-1}} - 1}{\frac{\gamma-1}{2}}} \qquad \text{(Eqn 1)}$$

The pitot-static probe gives the total and static pressures, P_t and P_0, respectively, and the ratio of specific heats, γ, is known to be 1.4 for air at the conditions in the inlet.

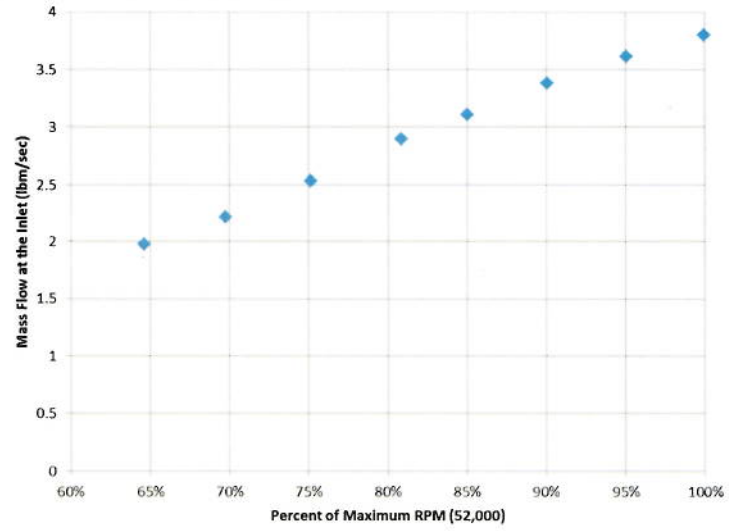

Figure 7. The installed mass flow of air at the inlet versus the percent of maximum RPM.[4]

The method used to determine the air mass flow rate of the installed engine included using pressure data obtained from a pitot-static probe placed in the inlet of the Chukar III. This pitot-static probe only returned data on the center of the flow however, therefore inducing some error into the air mass flow rate calculations which will be discussed further in results. Several key findings can be taken from last semester's efforts. First the corrected thrust at 100% RPM was found to be 232.5 lb_f[4] which represents a reduction of 3.1% from the published thrust of 240 lb_f.[1] Secondly the TSFC at 100% RPM was 1.154 lb_m/lb_f-hr[4] which is 3.8% better than the published TSFC of 1.2/hr.[1] This trend is the opposite of what would be expected for an installed performance parameter. The final takeaway from last semester's data was that the TSFC increased as the engine approached 100% RPM rather than continue its downward trend leveling off as it reached 100% RPM. This is most likely due to the increased Mach values at the

inlet of the aerial target drone, since inlet losses increase as the Mach in the inlet increases for a serpentine inlet. Another driving factor for the increase in TSFC at high engine speeds could be that by the design of the engine, the nozzle exit velocity, V_9, reaches the value for optimum propulsive efficiency, η_p, at 90-95% throttle, and the propulsive efficiency decreased as V_9 continued to increase with the increasing throttle setting. Since this project is evaluating the uninstalled performance of the engine, the intake of the drone will not be a factor in the TSFC; therefore, the TSFC is expected to decrease towards 100% RPM and level off rather than follow the trend experienced last semester if the inlet is main driving factor for the increase in TSFC at high engine speeds.

B. Objectives

The objective of this experiment is to compare engine performance for four cases: installed using the WJ24-8F engine data gathered during the Spring 2011 semester at the U.S. Air Force Academy, published data, uninstalled with a bell mouth inlet, and uninstalled without a bell mouth inlet. The WJ24-8F performance evaluation is being conducted in hopes that the engine will be validated as a test platform for future Air Force Academy research, and that methods for effectively testing and evaluating small scale turbojet engines will be developed. Performance parameters evaluated include thrust and TSFC, as well as the installed and uninstalled mass flow rate solved both analytically and experimentally. All compared experimental parameters are corrected to sea level conditions to mitigate the data fluctuations due to different test conditions.

II. Theory

A. Engine

The WJ24-8F is a small scale turbojet engine. The WJ24-8F was designed with two stages of compressors the first being an axial flow compressor stage and the second a centrifugal compressor stage.[4] The WJ24-8F also utilizes an annular combustor as well as a single turbine stage.[4] During operation, air flows through the inlet into the compressor stages; the two stages of compressor increase the pressure of the flow and condition it for the combustor. In the combustor fuel is mixed with roughly 40% of the air flow; this fuel air mixture is then ignited in order to expand the gasses and energize the flow. Once energized, the flow passes through the turbine where the energy required to run the compressor stages is extracted from the high energy flow. The flow then passes through the nozzle where it is accelerated and the remaining energy in the flow is translated into thrust.

B. Installed

Much of the installed engine performance is determined by the inlet of the engine since the airflow into the engine is determined by the inlet. The smoother the flow into the engine the more efficient the engine compressor stages will be, and therefore, the more efficient the engine will be. The ideal engine inlet geometry is a bell mouth which is large enough and has a smooth enough curve, to direct ambient air into the engine without causing any turbulence or vortices. Unfortunately, such inlets are only feasible on test stands. When an engine is put into service on an aircraft, many different factors influence the geometry of the inlet, only one of which is flow characteristics. Such is the case with the BQM-74 aerial target drone. Many design considerations led to a serpentine inlet design. This design experiences higher inlet losses than a straight inlet. This is due to the turning of the flow as it rounds the two bends in the serpentine inlet. As the flow turns at these bends two things occur. First at each turn the flow has an effective impact surface where the flow "hits a wall" as it is being turned. This increase in frictional effects causes losses in the inlet. Second, the turning of the flow causes a separation point after the turn since the flow cannot turn sharply enough to stay attached to the wall of the inlet. This effectively reduces the area of the inlet, since the flow cannot stay attached as it turns the corner; the flow only sees the area between the wall and the boundary layer of the separation point. Once again, this decreased area increases losses of the inlet. Fortunately, the serpentine inlet of the BQM-74 aerial target drone has a relatively mild design and therefore the installed losses are minimal. Figure 12 below depicts the installed inlet.

Figure 12. Installed inlet.[5]

Two points on the thrust curve were analytically examined to determine losses due to the serpentine inlet. 73% and 102% throttle were used in order to characterize the low and high ends of the thrust curve respectively. It was determined that the inlet caused roughly a 2 lbf thrust loss at 73% thrust and roughly a 15 lbf loss at 102%. This data seems to indicate that the performance losses due to the inlet increase as throttle increases; however, it is important to note that the inlet losses would be different in flight conditions than on a test stand since the test stand introduces losses such as *vena contracta* which would not be present at flight conditions.

C. Uninstalled With Bell Mouth

The ideal setup for an engine being bench tested requires a properly sized bell mouth inlet. The bell mouth inlet is ideal because flow cannot turn sharp corners and will separate restricting the area of the inlet seen by the flow. This separation effectively decreases the mass flow into the engine. An inlet with a gradual curve is needed to guide the flow into the engine smoothly, negating this effect. A properly sized bell mouth has no separation points or vortices at its lip and smoothly directs the flow into the compressor face with minimal losses. This allows the true performance capabilities of the engine to be observed and established as a baseline from which designers can estimate the amount of thrust they will get for a given installation configuration. Figure 13 below shows the bell mouth inlet configuration.

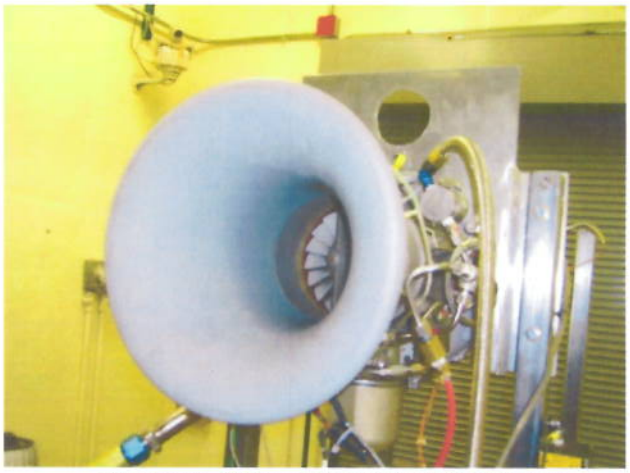

Figure 13. Bell mouth inlet configuration.

The addition of a bell mouth has other effects on data however. As the air begins to flow through the bell mouth to the engine, it transitions from static atmospheric conditions to the flow conditions needed by the engine. This means that the flow accelerates towards the engine. With the changing velocity of the flow comes changing static pressures. This means that the bell mouth experiences the same phenomena as the wing of an aircraft. On the inside of the bell mouth there is a relatively high speed flow over the surface with correspondingly lower static pressures, while on the exterior of the bell mouth there is static atmospheric conditions. This creates a pressure differential

precisely as the flow over a wing does. The pressure difference of the bell mouth creates "extra thrust" felt by the instruments. Figure 14 below depicts this phenomenon.

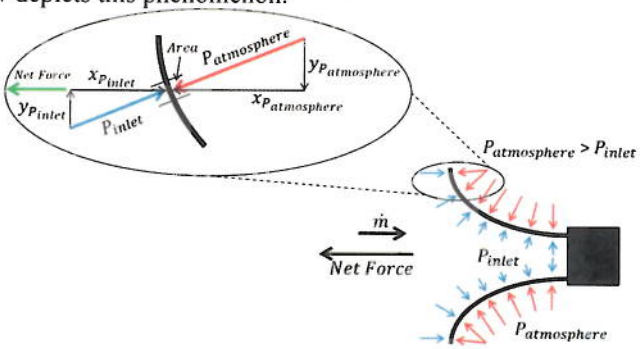

Figure 14. Additive net force due to pressure gradient along the bell mouth.

In order to measure the effects of this pressure differential on thrust readings, the pressure differential was solved using piece wise integration at 73% throttle and 102% corrected throttle. Several assumptions were made when solving for the pressure difference including an adiabatic, isentropic inlet with incompressible 1-D flow. While the max Mach number measured at the neck of the bell mouth of the high sample point tested was approximately M=0.35, and therefore slightly in the compressible regime, the majority of the flow through the bell mouth remained in the incompressible regime. The lower throttle setting test point never entered the compressible regime for air. The pressure at the static port ring was analytically calculated to be 10.38 psi using the incompressible bell mouth model for 102% throttle, while the experimentally measured static pressure was 10.35 psi in this case. The difference between the experimental results and the analytical model shows that the model's assumptions did affect the data solved for; however, the percent difference between these two pressures was found to be 0.28%. This difference was considered statistically negligible, and therefore, the model was validated.

The piecewise integration separated the interior of the bell mouth into twenty two distinct bands. Figure 15 below shows an example of how the bell mouth was broken into bands for piecewise integration. The static pressure experienced by each of the bands was solved for using Equation 2 and 3 below. In order to calculate the area each of these pressures affected, the circumference at each known point along the curve was calculated using Equation 3 and averaged with that of the next point. This allowed the average circumference of the two points to define the circumference of the band at each stage. The distance between points was then solved for using Equation 4.

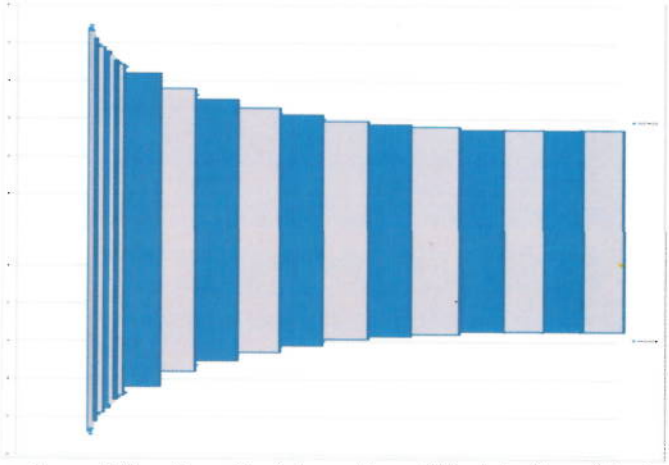

Figure 15. Example bands used for piecewise integration of the interior of the bell mouth; each axis is measured in inches and the bands are defined by the known points on the curve of the bell mouth.

$$\dot{m} = \rho A V \quad \text{(Eqn 2)}$$

$$P = P_t - \frac{1}{2}\rho V^2 \quad \text{(Eqn 3)}$$

$$Circumference = 2\pi r \quad \text{(Eqn 4)}$$

$$d = \sqrt{(x_2 - x_1)^2 + (y_2 - y_1)^2} \quad \text{(Eqn 5)}$$

The area of each band was determined by multiplying the band's average circumference by the distance between the two end points of the band. The pressure was then multiplied by said area to get the force acting normal to the surface of each band. After finding this force, the x-component was solved for using trigonometric relationships in order to find the force acting in the same axis as the thrust. The y-component of the force cancels itself out due to the symmetry of the bell mouth about the x-axis. The same process was then followed to find the opposing force on the exterior of the bell mouth. On the exterior however, only 12 bands were used since the exterior curve of the bell mouth is less aggressive and the pressure on the surface is constant at every point. When these forces are resolved, it is found that at 102% throttle on the 2 Dec test roughly 11.5 lbf of thrust were added by the bell mouth and that on the same test at 73% throttle roughly 0.901 lbf of thrust were added by the bell mouth. These figures were then corrected to sea level and it was determined that at 102% throttle 15.04 lbf of corrected thrust were added by the bell mouth and at 73% throttle 1.175 lbf of thrust were added by the bell mouth. These values highlight the key trend that the effects of the bell mouth pressure differential increase as throttle increases.

D. Uninstalled Without Bell Mouth

One main driver for performance differences between the two uninstalled cases (with and without the bell mouth inlet) is an effect called *vena contracta*. This effect is due to the fluid's (air's) inability to turn sharp corners at high velocities, and is mainly a function of the geometry of the inlet.[2] The inability to efficiently turn sharp corners leads to a total pressure drop across the inlet. This pressure loss is shown in the loss coefficient, K_L, which is defined in Equation 6 below.

$$K_L = \frac{\Delta p}{\frac{1}{2}\rho V^2} \quad \text{(Eqn 6)}$$

$$Re = \frac{\rho V D}{\mu} \quad \text{(Eqn 7)}$$

The actual value of K_L is strongly dependent on the geometry of the component considered. It may also be dependent on the fluid properties. That is, $K_L = \phi(geometry, Re)$ where Re, as defined in Equation 7, is the inlet Reynolds number. In the above equations ρ is the density of the fluid, $\Delta\rho$ is the change in density of the fluid, V is the velocity of the fluid, D is the hydraulic diameter of the inlet, and μ is the viscosity of the fluid. For many practical applications the Reynolds number is large enough so that the flow through the component is dominated by inertia effects, with viscous effects being of secondary importance.[2] This is true due to the relatively large accelerations and decelerations experienced by the fluid as it flows along the curved, variable-area path through the inlet. In a flow that is dominated by inertia effects rather than viscous effects the pressure drops usually correlate directly with the dynamic pressure. This is why the friction factor for very large Reynolds number fully developed flow is independent of the Reynolds number. Thus, in most cases of practical interest the loss coefficients for components are a function of geometry only, $K_L = \phi(\text{geometry})$.[2] As a rule of thumb, the lower the K_L value, the lower the associated loss is; therefore, lower K_L values are better for inlet and overall engine performance.

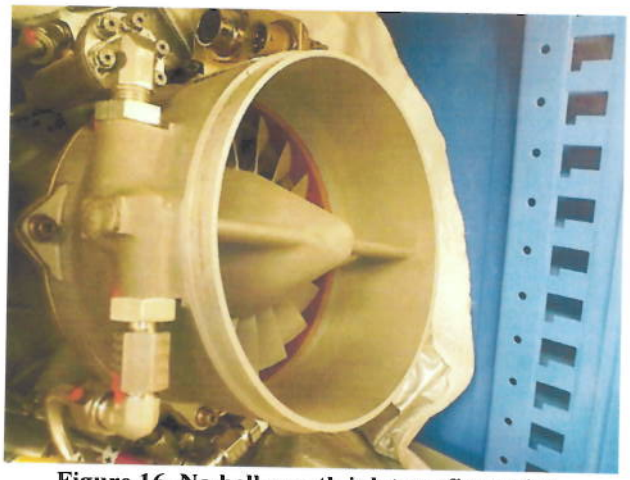

Figure 16. No bell mouth inlet configuration.

A *vena contracta* region may result because the fluid cannot turn a sharp right angle corner. The flow separates from the sharp corners shown in Figure 16 above. The maximum velocity at section (2) in Figure 17 below is greater than the velocity in the inlet at section (3), and the pressure there is lower. If this high-speed fluid could slow down

efficiently, the kinetic energy could be converted into pressure (the Bernoulli Effect), the ideal pressure distribution would result, and the head loss for the entrance would be essentially zero.[2]

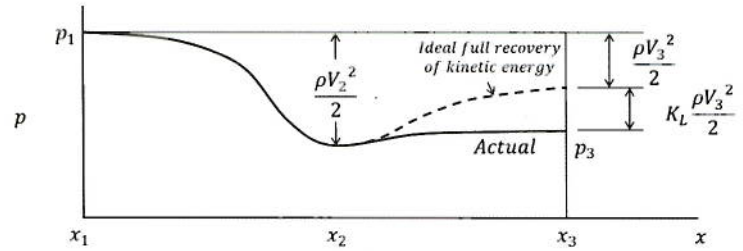

Figure 17. Flow pattern and pressure distribution for a sharp-edged entrance.[2]

Such is not the case. Although a fluid may be accelerated efficiently, it is very difficult to slow down (decelerate) a fluid efficiently. Thus, the extra kinetic energy of the fluid at section (2) of Figure 17 above is partially lost because of viscous dissipation, so that the pressure does not return to the ideal value. An entrance head loss (pressure drop) is produced as is indicated in Fig. 16. The majority of this loss is due to inertia effects that are eventually dissipated by the shear stresses within the fluid. Only a small portion of the loss is due to the wall shear stress within the entrance region. The net effect is that the loss coefficient for a square-edged entrance is approximately $K_L = 0.50$. One-half of a velocity head is lost as the fluid enters the inlet. Also, the effects of *vena contracta* for this case may be reduced by the compressor bearing housing geometry. This additional geometry increases the difficulty of the *vena contracta* analysis because it directs the flow outward and toward the compressor blades. This flow redirection should reduce the effects of *vena contracta* because the fluid is not required to decelerate as much as if the bearing housing was not present. Figure 18 below shows the flow separation and the reduction in effective inlet area.

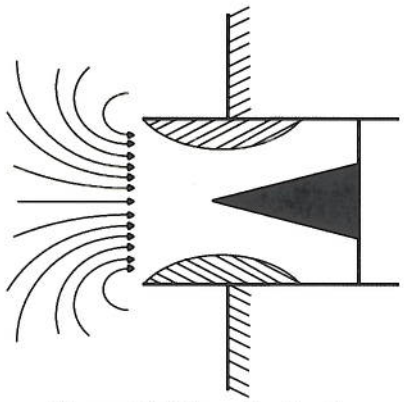

Figure 18. *Vena Contracta.*

When comparing the uninstalled engine thrust with a bell mouth inlet to the uninstalled thrust without a bell mouth inlet, it can be assumed that once the forces acting on the bell mouth are negated, any thrust deficit remaining would be due to the *vena contracta* phenomena. This thrust deficit was solved for at 73% throttle and 102% throttle. It was found that at 73% throttle approximately 8.66 lbf of thrust is lost to *vena contracta* while at 102% throttle only 3.17 lbf of thrust is lost to *vena contracta*. This seems to indicate that the effects of *vena contracta* decrease as throttle increases.

E. Corrected Parameters

Each test run is performed under differing conditions; therefore, it is necessary to correct the experimental data to sea-level conditions. While the test runs never exceeded 100% RPM, once these values are corrected to sea level some of the values do exceed the 100% RPM line. The corrections are based on the ratio between the test environment pressure and temperature, and the reference pressure and temperature. For this analysis, sea-level standard day conditions are used, which are defined as $P_{ref} = 14.696\,psia$ and $T_{ref} = 518.69\,R$. The corrected engine parameters are outlined in Table 19 below.

Table 19. Corrected engine parameters and their equations.[3]

Parameter	Symbol	Corrected Parameter
Total pressure	P_{ti}	$\delta_i = \frac{P_{ti}}{P_{ref}}$
Total temperature	T_{ti}	$\theta_i = \frac{T_{ti}}{T_{ref}}$
Rotational speed	$N = RPM$	$N_{ci} = \frac{N}{\sqrt{\theta_i}}$
Mass flow rate	$\dot{m}_i$	$\dot{m}_{ci} = \frac{\dot{m}_{ti}\sqrt{\theta_i}}{\delta_i}$
Thrust	F	$F_c = \frac{F}{\delta_0}$
Thrust-specific fuel consumption	S	$S_c = \frac{S}{\sqrt{\theta_0}}$
Fuel mass flow rate	$\dot{m}_f$	$\dot{m}_{fc} = \frac{\dot{m}_f}{\delta_2\sqrt{\theta_2}}$

III. Set-up and Procedure

A. Test Cell Setup

The Williams International WJ24-8F is mounted on a static thrust stand in the U.S. Air Force Academy, Department of Aeronautics Laboratory Test Cell #4. Figure 8 below depicts the thrust stand and engine setup. The engine is allowed limited movement in the direction of the thrust vector, but not in the lateral (side-to-side) or vertical (up and down) directions. The limited movement allowed is acceptable because the test stand is designed to require only minimal movement to gather load cell data. Furthermore, the resistance to movement offered by the test stand is considered negligible due to the low restriction and the calibration of the load cell. The load cell calibration is performed by placing a known set of weights on a nylon cable that is attached to the test stand along the thrust vector and centerline of the engine through the use of a single pulley. The *SuperFlow* data collection software is then calibrated to match the known weight values. The load cell itself is not along the centerline of the engine, and therefore creates a moment arm for the thrust to act about. This moment arm is taken into account in the calibration process; however, and the load cell calibration remains linear.

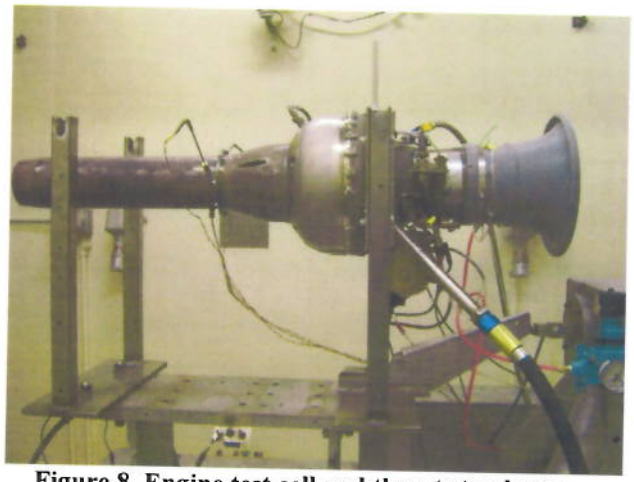

Figure 8. Engine test cell and thrust stand set up.

The WJ24-8F, in the testing configuration, consists of four main systems: lubrication, fuel, ignition, and air start. The engine itself is tested as delivered from Williams International, and includes the alternator and oiling system. In order to pre-lubricate the engine before startup, 100 psi externally compressed bleed air from the U.S. Air Force Academy Department of Aeronautics Test Cell #4 shop air is regulated to 10-12 psig and is connected to the engine's oil misting system through a check valve that will close when the engine is operating under its own power. In operating conditions, bleed air from the first stage axial compressor, which is around 18 psig, closes the aforementioned check valve and operates the oil misting system. This system simply uses compressed air to pressurize a small oil reservoir, which in turn continuously sprays a fine mist of oil on the bearings within the

engine. The reservoir lasts several test runs before requiring a refill, and includes a heater to bring the oil up to operating temperature.

To provide a fuel supply with a controllable fuel flow rate to the engine, a variable electric automotive fuel pump is used in conjunction with a power supply located in the test cell control room. This fuel pump draws JP-8, through a fuel filter, from a 10 gallon fuel tank located in the test cell, and routes the fuel to the pre-existing fuel system on the WJ24-8F. The fuel shutoff valve included on the WJ24-8F is retained in order to have complete control over the fuel flow to the engine in the case of an emergency. The fuel pump operates at multiple speeds and is controlled by the variable power supply located in the test cell control room. In essence, the fuel pump power supply is the throttle control for the engine. As voltage is increased from 3V to 10V, fuel flow increases from 98.82 lbm/hr to 417.12 lbm/hr, respectively. The lowest voltage setting possible for sustained engine operation is 5V. Above 5V the fuel flow meter calibration is nearly linear. Figure 9 below shows the fuel flow meter calibration against the fuel pump voltage setting, and Figure 10 depicts the fuel system.

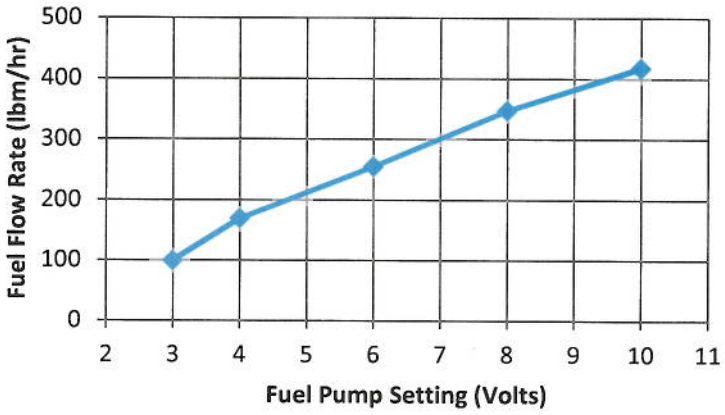

Figure 9. Fuel flow meter calibration curve.

Figure 10. Fuel system.

The ignition system consists of the T-63 ignition control module, the igniter, and the necessary connections between the *SuperFlow* console in the control room, the ignition control module, and the igniter. When the ignition switch is activated on the *SuperFlow* console in the test cell control room, the T-63 ignition control module is activated and energizes the igniter in the engine. The igniter is exposed directly to the air/fuel mix in the combustor, and when energized, creates a sufficient spark to ignite the air/fuel mix. An air start apparatus using bleed air from the trisonic wind tunnel air tanks is also connected to the engine. This air is regulated to roughly 250 psig. The air start apparatus consists of an electronically activated valve and high-pressure air hoses necessary to connect the compressed air supply to the valve, and the valve to the pre-existing air start port on the engine. The air start apparatus spools the engine up to starting RPM until the burner can ignite and the engine becomes self-sustaining.

The test setup includes an array of instrumentation equipment to gather the necessary data for analysis. The *SuperFlow* test cell box includes a thermocouple and pressure transducer to collect the test cell temperature and barometric pressure, respectively. A bell mouth is fitted to the engine which includes a static pressure port ring to collect inlet static pressure data. A thermocouple is attached to the exhaust housing in order to measure exhaust gas temperature data. The alternator included on the engine package is used to output frequency data that is, in turn, used to collect engine speed data. A frequency cable connects the alternator to a frequency channel on the *SuperFlow* test cell box. This frequency was calibrated to give accurate engine speed using an optical RPM measurement device. A pressure transducer attached to the compressor bleed air output is used to collect compressor pressure data. All data collection equipment is connected to the SuperFlow test cell box. The test stand is equipped with a load cell that is also connected to the SuperFlow test cell box. Figure 11 below lists the equipment used for the engine tests.

B. Test Procedures

Testing begins by following the safety/start-up checklist in Appendix A. Once all procedures are followed and the engine is operating at idle (42,000RPM), the power supply regulating the fuel pump voltage is reduced until engine speed reaches roughly 30,000 RPM. The engine is allowed to settle into steady state operation and then roughly twenty five seconds of data is taken at that single test point. The *SuperFlow* system continuously collects data at 1Hz. In an effort to reduce uncertainty data is collected for twenty five seconds at each test point to provide a quality sample for data reduction. Once roughly twenty five seconds of data have been taken at the first test point, the voltage is increased to increase the fuel flow, and thus the engine speed, until the next test point engine speed is reached. The engine is allowed to reach steady state operation, and another twenty five seconds of data is collected. This process is continued until the maximum engine speed (52,000 RPM) is reached. Once the maximum engine speed is reached the process is reversed, and data is collected following the same method outlined above. This deceleration is continued until the engine speed reaches roughly 30,000 RPM, then the voltage is reduced rapidly to zero, and the fuel shut-off button on the *SuperFlow* console is pressed to ensure the fuel supply is cut. Collecting data on both the acceleration and deceleration of the engine is beneficial for two reasons. First, it allows more data to be taken to improve the results, and secondly it allows for a cool down period without wasting valuable engine operation time. The WJ24-8F is designed to be expendable, thus it has a short life cycle, and collecting data on both the acceleration and deceleration phases of engine operation maximizes the data yield while minimizing the total engine test time.

IV. Results and Discussion

A. Uncertainty Analysis

An uncertainty analysis is performed after the five test runs are completed in conjunction with the data reduction process. The uncertainty in the experimental data comes from two distinct sources: bias and precision. Bias error is caused by the inherent error associated with any instrument, and is obtained from the manufacturer's specifications for the device. The bias error in this experiment is outlined in Figure 20 below. Precision error is caused by the unpredictable variation within the collected data samples. The precision error in this experiment is determined by finding two standard deviations from the average value of the collected data samples for each of the aforementioned test points. For the number of data points taken for each engine operating condition, a Student-T distribution, or two standard deviations, gives a 95% confidence interval for each point. Total uncertainty for each parameter is found using Equation 8.

Parameter	Bias Error
Engine Speed	± 100 RPM
Fuel Flow Rate	± 1.5 lbm/hr
Thrust	± 0.3 lbf
Temperature	± 2.0 °R

Figure 20. Test set up bias error.

$$U_{Total} = \sqrt{Bias^2 + Precision^2} \qquad \text{(Eqn 8)}$$

The above process is used to find the total uncertainty for the engine speed and thrust data samples, but a slightly different approach is required to find the total uncertainty for the thrust specific fuel consumption (TSFC) since TSFC is a calculated parameter, not a directly measured parameter like engine speed or thrust. Equations 9, 10, and 11 below are used to find the total uncertainty associated with TSFC. The corrected S is solved for using the equation in Figure 19.

$$S = \frac{\dot{m}_f}{F} \quad \text{(Eqn 9)}$$

$$S_{corrected} = \frac{S}{\sqrt{\theta_0}} \quad \text{(Eqn 10)}$$

$$U_{S_{corrected}} = \sqrt{\left(\frac{dS}{dF}B_F\right)^2 + \left(\frac{dS}{dF}P_F\right)^2 + \left(\frac{dS}{d\dot{m}_f}B_{\dot{m}_f}\right)^2 + \left(\frac{dS}{d\dot{m}_f}P_{\dot{m}_f}\right)^2 + \left(\frac{dS}{dT_t}B_{T_t}\right)^2 + \left(\frac{dS}{dT_t}P_{T_t}\right)^2} \quad \text{(Eqn 11)}$$

B. Performance Parameters

After the five separate test runs were conducted, three with the bell mouth and two without, the data was reduced, corrected to sea level, and uncertainty was calculated. The final data was then compiled into graphs in order to easily identify performance, error, and the differences between corrected and uncorrected data as well as to typify the difference between installed and uninstalled performance. The following graph, Figure 21, shows the corrected thrust values from each test against the percent maximum RPM.

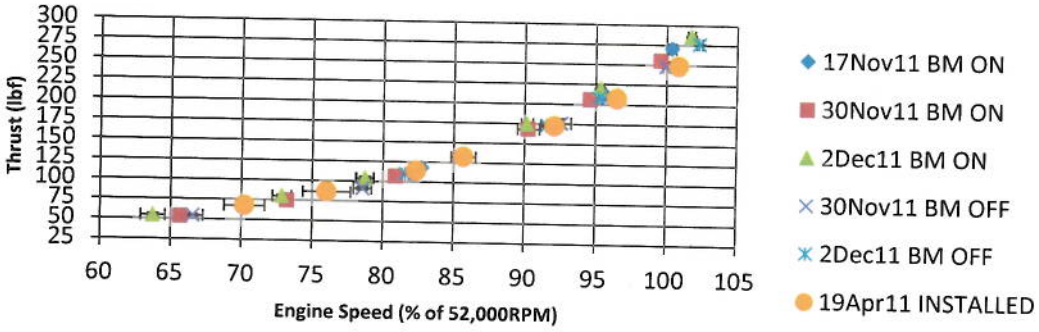

Figure 21. Corrected thrust versus percent maximum RPM (BM=Bell mouth); the error bars incorporate the bias error as well as the precision error of two standard deviations.

The corrected thrust at 100% RPM with the bell mouth installed was found to be about 260 lb_f which is 11.8% higher than the published data. Furthermore, this corrected thrust represents a 16.2% increase between this experiment and those conducted on the installed engine. After reducing and correcting the thrust data, the TSFC and the mass flow rate through the engine were calculated. The TSFC at 100% RPM was found to be approximately 1.15 lb_m/lb_f-hr. This is 4.2% higher than the published data as well as a 18.3% higher than the installed data.

The corrected thrust and TSFC obtained from the experimentation are better than the expectations of installed vs. uninstalled performance parameters. While it is expected for uninstalled thrust to be better than installed thrust, it would be expected that the corrected thrust should align closely to the published uninstalled value. This mark, however, was exceeded by roughly 8%. Once again, it is expected that the uninstalled TSFC meets the published value; however, in these tests the engine performed with 4.2% higher TSFC than the published values. This is most likely due to the fact that the published data correlates with the engine performance towards the end of the engine life cycle. The engine used for testing is very well kept in comparison to an installed and operational engine; therefore, better than published results are expected.

One particular trend that should be noted is that the TSFC begins to level out as it reaches 90-95% RPM. This flattening out or stabilizing is what should occur when the engine reaches its maximum output and stabilizes there. However, the data also shows an increase in TSFC as the engine approached 100% RPM. This difference can most directly be attributed to the relationship between thermodynamic and propulsive efficiency. As the engine speed is increased the thermodynamic efficiency of the engine increases. While the thermodynamic efficiency is increasing in the engine, the propulsive efficiency is decreasing. This occurs because the velocity of the exhaust from the engine, V_9, is increasing while the engine itself remains static. Before the 90% to 95% engine speed range, the increase in thermodynamic efficiency is greater than the decrease in propulsive efficiency, so the TSFC decreases.

After the 90% to 95% engine speed range, however, the losses in propulsive efficiency begin to outweigh the increase in thermodynamic efficiency and the TSFC begins to increase again. These trends can be seen in Figure 21below.

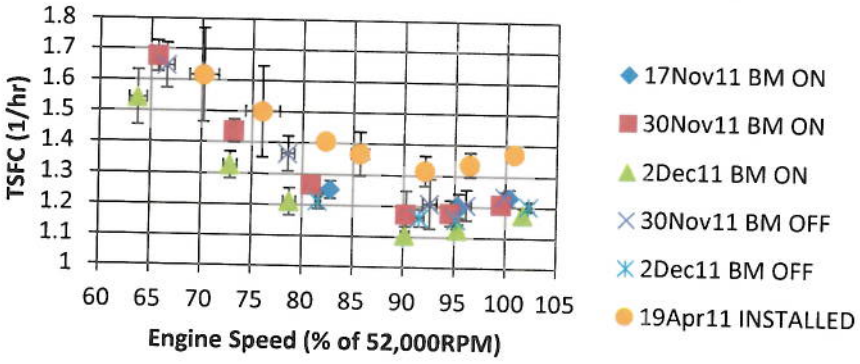

Figure 22. Corrected thrust specific fuel consumption versus percent maximum RPM (BM=Bell mouth); the error bars incorporate the bias error as well as the precision error of two standard deviations.

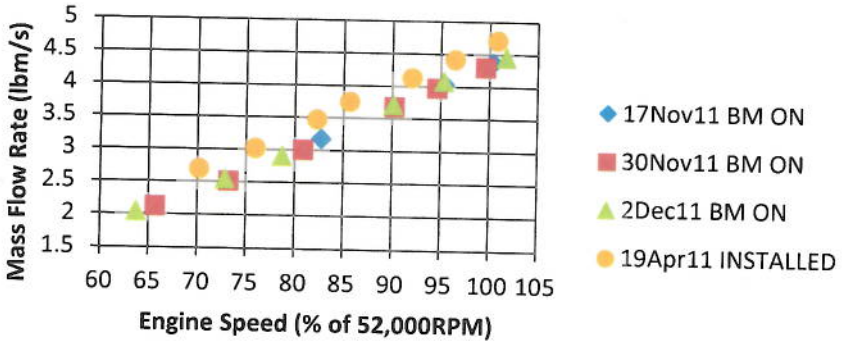

Figure 23. Corrected mass flow rate versus percent maximum RPM (BM=Bell mouth).

The air mass flow rate results shown in Figure 23 above are mainly used for comparison purposes in this project; however, the air mass flow rates may be of importance in future research. As previously mentioned, the installed air mass flow rate was determined using a pitot-static probe placed in the installed serpentine inlet. This set up only returns the pressure of the flow in the center of the engine and so may not truly represent the pressure trends in the inlet. Furthermore, the effects of *vena contracta* were not evaluated for the installed cases; therefore, the effective inlet area was not considered and the resulting air mass flow rates are higher than expected. For the uninstalled cases, the air mass flow rate is determined using the static pressure ports on the bell mouth inlet as well as the total barometric pressure in the test cell. The bell mouth inlet negates most of the possible reductions in effective inlet area due to separate or turbulent flow. This difference in pressure data acquisition methods between the installed and uninstalled cases results in the difference between the installed and uninstalled air mass flow rates, and the uninstalled test set up to determine air mass flow rate tends to yield more accurate results. The air mass flow rates are corrected to sea-level conditions using the air mass flow rate correction equation in Figure 19 above. Unfortunately, since the static pressure ports are built into the bell mouth inlet, the tests without the bell mouth yield no inlet static pressure data; therefore, the air mass flow rate cannot be determined with the described setup.

In order to simplify the comparison of the three test cases, smooth curves for thrust and TSFC are plotted in Figure 24 and Figure 25, respectively. Figure 24 shows the corrected thrust for the two uninstalled cases, as well as the installed configuration. The corrected thrust for the uninstalled with bell mouth inlet configuration is roughly 5.9% higher than for the uninstalled without a bell mouth case, and over 10% higher than for the installed configuration. The WJ24-8F does produce more thrust in the installed configuration than the uninstalled without a bell mouth inlet configuration between 65% and 90% engine speed. This occurs because at lower engine speeds, the effects of *vena contracta* dominate the losses while at higher engine speeds the losses associated with the serpentine inlet dominate.

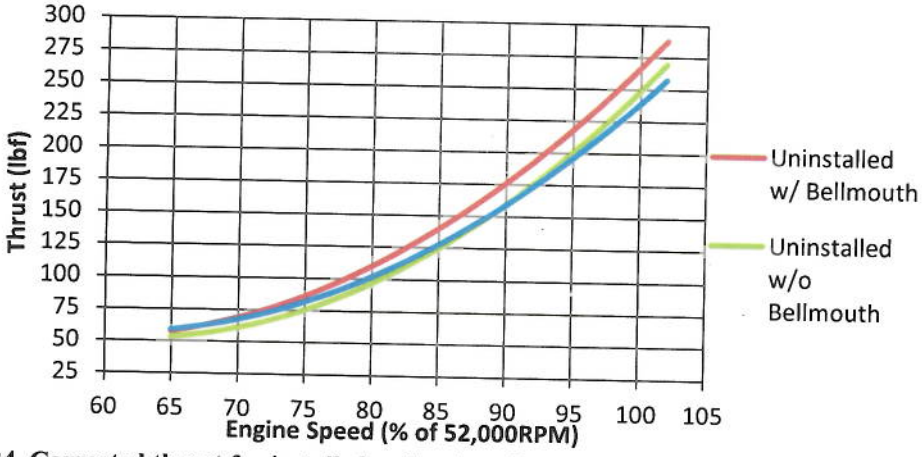

Figure 24. Corrected thrust for installed and uninstalled engines (with and without bell mouth).

Figure 25 below represents the differences between the efficiencies of the three tested configurations. As expected, the bell mouth configuration yielded the best TSFC, which is 6.7% better than without a bell mouth inlet and 17.5% better than when installed.

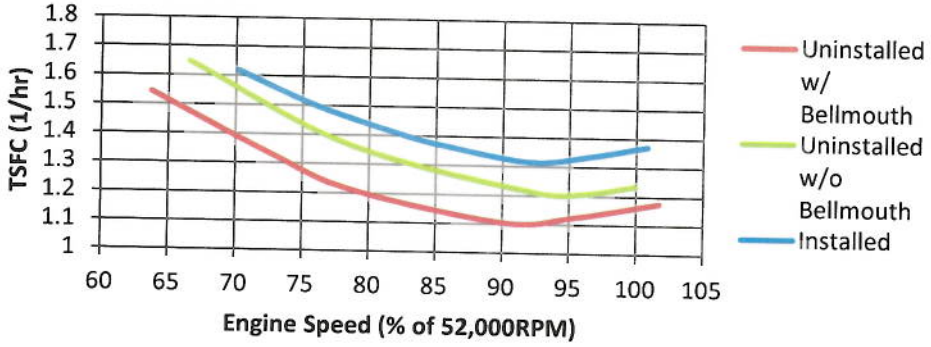

Figure 25. Corrected TSFC for installed and uninstalled engines (with and without bell mouth).

V. Conclusion

The Williams International WJ24-8F turbojet engine was tested over the course of five test runs, three with a bell mouth inlet, and two without. After reducing the data from these test runs, the engine parameters at military power are corrected to sea level. Several important trends can be gleaned from these results. The test results and corresponding trends are outlined in Figure 26 below.

Table 26. Corrected thrust values and percent differences for each engine test configuration.

Test Set-Up	Corrected Thrust	Difference from published data
Uninst. w/ BM	260 lbf	8.33%
Uninst w/o BM	245 lbf	2.1%
Installed	235 lbf	2.1%
Published	240 lbf	True value

Each of the percent differences outlined above have different likely causes. The corrected thrust for the bell mouth inlet configuration is most likely higher than that of the configuration without a bell mouth inlet due to a mixture of the pressure differential acting on the bell mouth and the *vena contracta* effect acting on the engine when the bell mouth is not present. The installed corrected thrust is most likely lower than the uninstalled configuration with a bell mouth inlet because the bell mouth configuration has the benefit of the pressure differential acting on the

inlet; furthermore, the installed engine has to cope with inlet losses due to its serpentine inlet which lower its thrust values, especially at military power. Finally, the uninstalled data for the bell mouth engine configuration is likely higher than the published value not only because of the pressure differential acting on the bell mouth, but also because when the manufacturer publishes its thrust value the engine must be able to maintain said thrust at the end of its life cycle, even after repeated thermal shock. It is therefore safe to assume the engine performance will be better than the published data during its life cycle while properly maintained in a test environment. It is important to note, that while the uninstalled corrected thrust without a bell mouth inlet was higher than the installed thrust at military power, it is actually lower than the installed values from roughly 65% to 90% throttle. This trend can best be explained by the phenomena of *vena contracta*. At lower throttle settings the losses due to *vena contracta* are greater for the uninstalled test configuration without a bell mouth inlet than the losses caused by the serpentine inlet of the Chukar III; however, as throttle exceeds 90%, the inlet losses due to the serpentine geometry of the Chukar III exceed the losses due to *vena contracta* effects on the uninstalled engine. The effects of the bell mouth additive force, *vena contracta*, and inlet losses were analytically determined at two engine speeds and are outlined below in Figure 27.

Test Configuration	73% Corrected Throttle (77.2 lbf thrust)	Percent of thrust	102% Corrected throttle (272.6 lbf thrust)	Percent of thrust
Thrust added by bell mouth inlet	1.18 lbf	1.53%	15.0413 lbf	5.52%
Thrust lost due to *vena contracta*	8.66 lbf	12.64%	3.17 lbf	1.18%
Thrust lost due to serpentine inlet	2.13 lbf	2.84%	15.36 lbf	5.97%

Figure 27. Effects of bell mouth inlet, *vena contracta*, and inlet losses at 73% and 102% throttle.

After calculating the corrected TSFC of the different engine configurations, the TSFC for each test configuration and its associated trends were outlined in Figure 28 below. The same reasons that corrected thrust varied apply here. However, it is of particular importance to remember that the WJ24-8F is a short life cycle engine that is designed to take repeated abuse to include landing in the ocean and being re-used. The abuse this engine takes as part of its mission requirements necessitates a durable and robust design; therefore, it is not surprising that a well maintained WJ24-8F engine relatively young in its life cycle would exceed its published performance parameters. One particular trend that should be noted is that the TSFC begins to level out as it reaches 90-95% RPM. This flattening out or stabilizing is what should occur when the engine reaches its maximum output and stabilizes there. The data actually shows an increase in TSFC as it approached 100% RPM. This difference can most directly be attributed to the tradeoff between thermodynamic and propulsive efficiencies. These results are due to the engine being mounted on a thrust stand and the abovementioned trends would be somewhat different if the engine was experiencing flight conditions since the velocity of the exhaust gas, V_9, would be closer to the Chukar III's velocity.

Table 28. Corrected TSFC values and percent differences for each engine test configuration.

Test Set-Up	Corrected Thrust	Difference from published data
Uninst. w/ BM	1.15/hr	4.2%
Uninst w/o BM	1.23/hr	2.5%
Installed	1.37/hr	14.2%
Published	1.2/hr[1]	True value

Finally, the mass flow rate of air through the engine was characterized and can be referenced in Figure 23. This data correlated well with previous research. Given the above findings, and their correlation with both published data and the previous research on the installed engine, it is believed that the WJ24-8F is reliable and proven enough to be used in future research as a test bed for other projects such as the Air Force Academy's ongoing endeavors in unmanned aerial systems and ejector theory. As such, all objectives for this project have been met or exceeded.

Acknowledgments

The team would like to thank our technician, Mr. Jerry Stermer, for his outstanding work and dedicated support of our project from its inception to its completion. Nothing would have been possible without him. The team would also like to thank Mr. Brian Kinsey and Mr. Jeffrey Falkenstine for their design and construction of the bell mouth inlet. Their unending support for this project and selfless dedication to its completion were instrumental at every stage.

References

[1]"Chukar III," *Northrop Grumman*, http://www.as.northropgrumman.com/products/targets_chukar3/asets/Chukar-III-DS-05.pdf [retrieved 20 January 2012].

[2]Fox, Robert W. and McDonald, Alan T., *Introduction to Fluid Dynamics*, Wiley, New York, NY, 1985.

[3]Mattingly, Jack D., *Elements of Propulsion: Gas Turbines and Rockets*, American Institute of Aeronautics and Astronautics, Inc., Reston, VA, 2006.

[4]McMullen, K. and Pichkur, D., "CAMPUS 2.0 Engine Performance Evaluation," Department of Aeronautics, U.S. Air Force Academy, CO.

[5]McMullen, K., and Pichkur, D., "CAMPUS 2.0 Engine Performance Evaluation Final Briefing," Department of Aeronautics, U.S. Air Force Academy, CO.

[6]Wheeler, Anthony J. and Ganji, Ahmad R., *Introduction to Engineering Experimentation*. 3rd ed. Boston, MA: Prentice Hall, 2010. Print.